

# Hybridization of topological surface states with a flat band

Sergey S. Krishtopenko,<sup>1,2</sup> Mauro Antezza,<sup>1,3</sup> and Frédéric Teppe<sup>1,\*</sup>

<sup>1</sup>*Laboratoire Charles Coulomb (L2C), UMR 5221 CNRS-Université de Montpellier, F- 34095 Montpellier, France*

<sup>2</sup>*Institute for Physics of Microstructures RAS, GSP-105, Nizhni Novgorod 603950, Russia.*

<sup>3</sup>*Institut Universitaire de France, 1 rue Descartes, F-75231 Paris Cedex 05, France*

(Dated: March 26, 2025)

We address the problem of hybridization between topological surface states and non-topological flat bulk band within an analytical Hamiltonian linear in quasimomentum. Our model is based on a mixture of the three-dimensional Bernevig-Hughes-Zhang and the two-dimensional pseudospin-1 Dirac-Weyl Hamiltonian, hence it also includes the case of HgTe-class and Cd<sub>3</sub>As<sub>2</sub> crystals at given hybridization strength. We show that hybridization with a bulk band in HgTe transforms initial Dirac-like surface states into two branches below the flat band and above the edge of conduction band. Dispersion of the lower branch depends on hybridization strength, while the upper branch always remains "massive" for any hybridization strength. By varying the position of the bulk flat band, we obtain a picture of the surface states for topological insulators and the appearance of the Fermi arcs for Dirac semimetals based on HgTe and Cd<sub>3</sub>As<sub>2</sub> crystals at different strength of hybridization.

## I. INTRODUCTION

The physics of topological materials is one of the most active areas in modern condensed matter research. It starts from Kane and Mele<sup>1</sup>, who identified a new type of topological property characterizing two-dimensional (2D) insulators, different from the property of the integer quantum Hall effect<sup>2</sup>. Later, these ideas have been generalized to a three-dimensional (3D) material<sup>3</sup>, yielding a family of topological insulators (TIs). The non-trivial topology of TIs arises from inversion between two bands with opposite parity resulting in gapless states at the boundaries, which are robust against disorder and contamination<sup>4-7</sup>. 2D TIs are characterized by 1D gapless edge states, where opposite spin states counter-propagate. On the other hand, 3D TIs are characterized by helical surface states consisting of a single Dirac cone, where the spin points perpendicular to the momentum. So far, both 2D and 3D TIs have been realized in many 2D systems<sup>8-14</sup> and bulk materials<sup>15-22</sup>.

Many materials with inverted band structure as it is in TIs, however, are bulk metals with the helical surface states. The prominent example is the HgTe-class materials, in which inversion between  $|\Gamma_6, \pm 1/2\rangle$  electron and  $|\Gamma_8, \pm 1/2\rangle$  light-hole bands originates 2D TI state in HgTe/CdTe quantum wells (QWs)<sup>8,9</sup>. The presence of an additional heavy-hole band  $|\Gamma_8, \pm 3/2\rangle$  makes HgTe a bulk semimetal since the  $\Gamma_8$  bands at the  $\Gamma$  point of the Brillouin zone are fourfold degenerate as  $J = 3/2$  multiplet. External tensile biaxial strain opens the gap between conduction  $|\Gamma_6, \pm 1/2\rangle$  and valence  $|\Gamma_8, \pm 3/2\rangle$  bands resulting in 3D TI state in HgTe crystal<sup>23,24</sup>.

However, an expected crossing point at  $k = 0$  of the Dirac surface states in HgTe-based 3D TI also lies below the edge of  $|\Gamma_8, \pm 3/2\rangle$  band. Therefore, these topological surface states, originating from the inversion between  $|\Gamma_6, \pm 1/2\rangle$  and  $|\Gamma_8, \pm 1/2\rangle$  bands, are hybridized with the heavy-hole band at non-zero quasimomentum  $k$ . The latter means that the surface states in the pres-

ence of hybridization with the "parasitic" bulk band may differ significantly from simple Dirac-like surface states of "conventional" 3D TI. The similar effect has been demonstrated recently for the Dirac-like edge states in 2D TI<sup>25,26</sup>.

In the opposite case, when  $|\Gamma_8, \pm 3/2\rangle$  band lies above the edge of conduction  $|\Gamma_6, \pm 1/2\rangle$  band, these two bands touch at certain points of the Brillouin zone and are presented as two highly anisotropic and tilted cones. This situation is realized in compressively strained HgTe films<sup>27</sup> and unstrained Cd<sub>3</sub>As<sub>2</sub> crystals<sup>28-31</sup>, which are known to be 3D Dirac semimetals<sup>32-34</sup>. The whole picture of the surface states is even more complex. On one hand, inversion between  $|\Gamma_6, \pm 1/2\rangle$  and  $|\Gamma_8, \pm 1/2\rangle$  bands should produce Dirac-like surface states of "conventional" 3D TI. On the other hand, the bulk nodes in 3D Dirac semimetals, projected on the given surface boundary, should be connected by two Fermi arcs<sup>32</sup>, which are nothing but the energy contour of the surface states. Thus, one cannot ignore the effect of hybridization with heavy-hole  $|\Gamma_8, \pm 3/2\rangle$  band on the surface states in Cd<sub>3</sub>As<sub>2</sub> and HgTe-based 3D Dirac semimetals.

So far, modification of the surface states by hybridization with bulk bands was studied only by the first-principles band-structure calculations<sup>29,35-37</sup>. It was shown that the helical surface states in bulk crystals may be pushed away from overlapping in momentum and energy with the parasitic bulk band. Moreover, the hybridization may lead to multiplied surface-state bands, in all cases retaining the helical characteristic<sup>35</sup>. All this possible scenarios in different bulk crystals motivate us to address the problem of hybridization between topological surface states and non-topological "parasitic" bulk band within simple analytical model.

In order to get a better understanding of the hybridization effect on topological surface states, we consider a simple "modified" 6-band Hamiltonian by admixing 3D Bernevig-Hughes-Zhang (BHZ) model<sup>16</sup> and

2D pseudospin-1 Dirac-Weyl Hamiltonian (cf. Refs<sup>38,39</sup>). Such analytical model allows explicitly treating an evolution of topological surface states by continuously changing of hybridization between the inverted bands and "parasitic" flat band in the bulk. The latter is hard to realize in the first-principles calculations<sup>29,35-37</sup>. At certain value of the parameter describing hybridization with the flat bulk band, our model also includes the case of Kane fermions<sup>40,41</sup> known for HgCdTe crystals. Within the proposed model, we explore an evolution of topological surface states in bulk HgTe at different strength of hybridization with the flat band. By varying position of this band relatively to the conduction band, we also obtain a picture of topological surface states in 3D TI and Dirac semimetals in strained HgTe films<sup>23,24,27</sup> and Cd<sub>3</sub>As<sub>2</sub> crystals<sup>28-31</sup>.

The paper is organized as follows. A general analytical model based on a mixture of the 3D BHZ and 2D pseudospin-1 Dirac-Weyl Hamiltonian is introduced in Section II. Section III contains discussion of topological surface states at different hybridization strength with the flat band. A picture of the surface states for 3D TIs and Dirac semimetals based on HgTe and Cd<sub>3</sub>As<sub>2</sub> crystals for different crystallographic orientations of topological boundary is also presented therein. The main results of this work are summarized in Section IV.

## II. THEORETICAL MODEL

We first introduce a "modified" 6-band Hamiltonian including a variable hybridization with the parasitic bulk band:

$$\hat{H} = \begin{pmatrix} \hat{H}_0(k_x, k_y) & \hat{H}_z(k_z) \\ \hat{H}_z(k_z)^\dagger & \hat{H}_0^*(-k_x, -k_y) \end{pmatrix}, \quad (1)$$

where the asterisk stands for complex conjugation and "†" corresponds to Hermitian conjugation. The blocks  $\hat{H}_0(k_x, k_y)$  and  $\hat{H}_z(k_z)$  in Eq. (1) are written as follows

$$\hat{H}_0 = \begin{pmatrix} C + M & \hbar v_{\parallel} k_{+} \sin \alpha & \hbar v_{\parallel} k_{-} \cos \alpha \\ \hbar v_{\parallel} k_{-} \sin \alpha & C + S & 0 \\ \hbar v_{\parallel} k_{+} \cos \alpha & 0 & C - M \end{pmatrix}, \quad (2)$$

$$\hat{H}_z = \begin{pmatrix} 0 & 0 & \hbar v_{\perp} k_z \\ 0 & 0 & 0 \\ \hbar v_{\perp} k_z & 0 & 0 \end{pmatrix}. \quad (3)$$

Here  $k_{\pm} = k_x \pm ik_y$ , where  $k_x$ ,  $k_y$ , and  $k_z$  are projections of quasimomentum onto given axis. In Eqs. (2) and (3),  $C$  represents the set of zero energy,  $S$  describes the position of parasitic flat band,  $v_{\parallel}$  and  $v_{\perp}$  are the values of velocity for the massless particles, which is anisotropic in general. Here,  $x$ ,  $y$  and  $z$  axes are oriented along (100), (010) and (001) crystallographic directions, respectively. For simplicity, we further assume  $v_{\parallel} = v_{\perp} = v$ <sup>41</sup>. The mass parameter  $M$  describes inversion of the bands with

opposite parity:  $M > 0$  corresponds to a trivial state, while  $M < 0$  stands for the band inversion<sup>8,16</sup>.

An important quantity of  $\hat{H}_0$  is the parameter  $\alpha$ , which describes the hybridization of the topological surface states with "parasitic" bulk flat band. An exact  $\alpha$  value for a given system can be obtained by k-p perturbation theory up to linear-in- $k$  order developed in the vicinity of critical point of the Brillouin zone by considering all the symmetries in the point group of bulk crystal. For instance, the Hamiltonian in Eq. (1) at  $\alpha = \pi/3$  is nothing but 6-band Kane Hamiltonian, which describes band structure in the vicinity of the  $\Gamma$  point in the crystals with zinc blend structure. Thus, depending on  $\alpha$ , our linear model consider different cases, interpolating between 3D BHZ model with decoupled flat band at  $\alpha = 0$  for Bi<sub>2</sub>Se<sub>3</sub>-class materials<sup>16</sup> and the Kane Hamiltonian at  $\alpha = \pi/3$ . Note that  $\hat{H}(\alpha)$ ,  $\hat{H}(-\alpha)$  and  $\hat{H}(\pi/2 \pm \alpha)$  are related by unitary transformation. Additionally, one can see that  $\hat{H}_0$  is nothing but the  $\alpha$ - $T_3$  model proposed by Raoux *et al.*<sup>39</sup>.

The Hamiltonian in Eq. (1) has three eigenvalues, each doubly degenerate owing to the time-reversal symmetry. The eigenvalues  $E$  obey the following equation:

$$\hbar^2 v^2 (k_x^2 + k_y^2) (E_{hh} \cos^2 \alpha + E_{lh} \sin^2 \alpha) + \hbar^2 v^2 k_z^2 E_{hh} = E_c E_{hh} E_{lh}, \quad (4)$$

where  $E_c(E) = C + M - E$ ,  $E_{hh}(E) = C + S - E$  and  $E_{lh}(E) = C - M - E$ .

In the particular case of unstrained crystals<sup>41</sup>,  $S = -M$ , and Eq. (4) provides an energy dispersion, which is independent of  $\alpha$ :

$$E = C \pm \sqrt{M^2 + \hbar^2 v^2 (k_x^2 + k_y^2) + \hbar^2 v^2 k_z^2}, \quad (5)$$

$$E = C - M.$$

Since the band dispersion is generally anisotropic and depends on the hybridization parameter  $\alpha$ , the picture for the surface states should be different for the boundaries parallel to the  $x$ - $y$  and  $x$ - $z$  planes.

To obtain dispersion of topological surface states, we further consider a junction with a trivial material (like CdTe), at which the mass parameter  $M$  changes its sign. Let us also assume that parameters  $C$  and  $S$  are functions of coordinates. In this case, Hamiltonian in Eq. (1) is Hermitian even in the presence of junction, when the operators  $\hat{k}_x$ ,  $\hat{k}_y$  and  $\hat{k}_z$  do not commute. We also consider  $v$  to be independent of coordinate assuming the same value from both side of the boundary. The latter, for instance, holds the boundary between trivial CdTe and non-trivial HgTe materials<sup>41</sup>. The values of  $\alpha$  are also supposed to be the same from both side of topological junction.

After some procedures, the initial Schrödinger equation with  $6 \times 6$  Hamiltonian  $\hat{H}$  is reduced to the eigenvalue problem for two spin states with the  $2 \times 2$  energy-dependent Hamiltonian  $\hat{H}_E$  containing the right order of

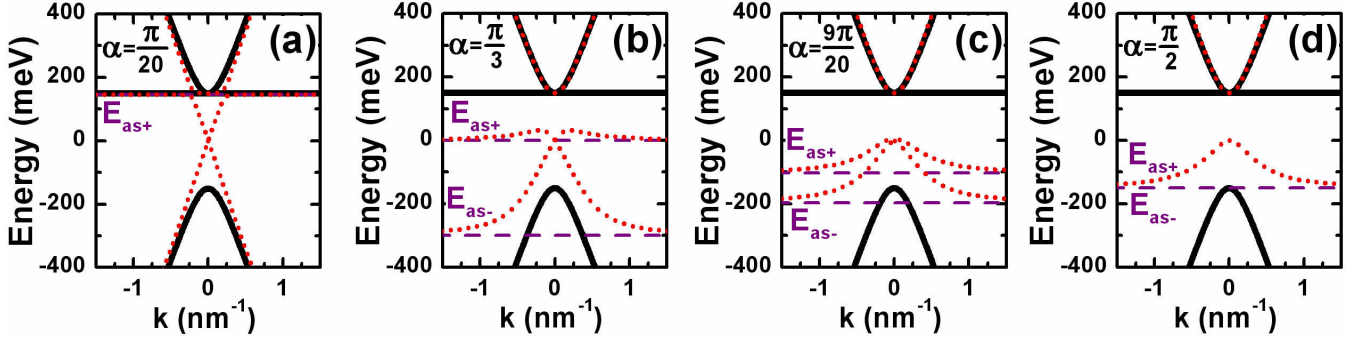


FIG. 1. (Color online) Dispersion of the bulk (solid black,  $k_z = 0$ ) and surface (dotted red) states as a function of  $k$  (where  $k^2 = k_x^2 + k_y^2$ ) for unstrained film ( $S^{(II)} = -M^{(II)}$ ) with parameters of HgTe sandwiched between CdTe layers at different strength of hybridization with the flat bands: (a)  $\alpha = \pi/20$ , (b)  $\alpha = \pi/3$ , (c)  $\alpha = 9\pi/20$ , (d)  $\alpha = \pi/2$ . The boundary is parallel to (001) crystallographic plane. The dashed purple lines represent the asymptotic energies  $E_{as\pm}$  at large  $k$ , given by Eq. (15). The value of  $\alpha = \pi/3$  corresponds to 6-band Kane Hamiltonian for band structure in HgCdTe crystals<sup>40,41</sup>.

non-commuting operators:

$$\begin{pmatrix} \hat{A} + i\hat{B} - E & \hat{K} \\ \hat{K}^\dagger & \hat{A} - i\hat{B} - E \end{pmatrix} \begin{pmatrix} \Phi_1(x, y, z) \\ \Phi_2(x, y, z) \end{pmatrix} = 0, \quad (6)$$

where  $E$  is the eigenvalue, and

$$\hat{A} = E_c - \hbar^2 v^2 \hat{k}_z \frac{1}{E_{lh}} \hat{k}_z - \hbar^2 v^2 \hat{k}_x \left( \frac{\cos^2 \alpha}{E_{lh}} + \frac{\sin^2 \alpha}{E_{hh}} \right) \hat{k}_x - \hbar^2 v^2 \hat{k}_y \left( \frac{\cos^2 \alpha}{E_{lh}} + \frac{\sin^2 \alpha}{E_{hh}} \right) \hat{k}_y, \quad (7)$$

$$\hat{B} = \hbar^2 v^2 \hat{k}_y \left( \frac{\cos^2 \alpha}{E_{lh}} - \frac{\sin^2 \alpha}{E_{hh}} \right) \hat{k}_x - \hbar^2 v^2 \hat{k}_x \left( \frac{\cos^2 \alpha}{E_{lh}} - \frac{\sin^2 \alpha}{E_{hh}} \right) \hat{k}_y, \quad (8)$$

$$\hat{K} = \hbar^2 v^2 \hat{k}_z \frac{\cos \alpha}{E_{lh}} \hat{k}_- - \hbar^2 v^2 \hat{k}_- \frac{\cos \alpha}{E_{lh}} \hat{k}_z. \quad (9)$$

Here, we keep previous notations, and  $E_c$ ,  $E_{hh}$  and  $E_{lh}$  are the same as for Eq. (4).

### III. RESULTS AND DISCUSSION

#### A. Surface states for the boundary parallel to (001) crystallographic plane

Let us now consider an abrupt semi-infinite boundary parallel to (001) crystallographic plane placed at  $z = 0$  ( $x$ - $y$  plane). In this case,  $k_x$  and  $k_y$  are good quantum numbers due to translation symmetry, and the wave-function of the surface states localized in the vicinity of  $z = 0$  has the form  $\Phi_{1,2}^{(I)} \sim \exp(\lambda_z^{(I)} z) \exp(ik_x x + ik_y y)$  for the region I,  $z < 0$  and  $\Phi_{1,2}^{(II)} \sim \exp(-\lambda_z^{(II)} z) \exp(ik_x x + ik_y y)$  for the region II,  $z > 0$ . Without loss of generality, we assume

that the region I correspond to CdTe with  $M^{(I)} > 0$ , while the region II is for HgTe and  $M^{(II)} < 0$ . By using given trial functions, one can find from Eq. (6) the values of  $\lambda_z^{(I)}$  and  $\lambda_z^{(II)}$ :

$$\lambda_z^{(n)} = \sqrt{k^2 \left( 1 + \frac{E_{lh}^{(n)} - E_{hh}^{(n)}}{E_{hh}^{(n)}} \sin^2 \alpha \right) - \frac{E_c^{(n)} E_{lh}^{(n)}}{\hbar^2 v^2}}, \quad (10)$$

where  $n = I, II$  and  $k^2 = k_x^2 + k_y^2$ . Note that Eq. (10) can be also derived from Eq. (4) by formal substitution  $-k_z^2 \rightarrow \lambda_z^2$ .

One can show that the following functions should be continuous across the junction:

$$\begin{pmatrix} \Phi_1 \\ \Phi_2 \end{pmatrix}, \quad \begin{pmatrix} \frac{1}{E_{lh}(E)} \frac{\partial}{\partial z} & -ik_- \frac{\cos \alpha}{E_{lh}(E)} \\ ik_+ \frac{\cos \alpha}{E_{lh}(E)} & \frac{1}{E_{lh}(E)} \frac{\partial}{\partial z} \end{pmatrix} \begin{pmatrix} \Phi_1 \\ \Phi_2 \end{pmatrix}. \quad (11)$$

The last boundary condition is obtained after integrating Eq. (6) across the small region in the vicinity of  $z = 0$ .

Applying these boundary conditions to  $\Phi_{1,2}^{(I)}$  and  $\Phi_{1,2}^{(II)}$ , the secular equation for the non-trivial solution leads to

$$\left( \lambda_z^{(I)} E_{lh}^{(II)} + \lambda_z^{(II)} E_{lh}^{(I)} \right)^2 = \left( E_{lh}^{(II)} - E_{lh}^{(I)} \right)^2 k^2 \cos^2 \alpha. \quad (12)$$

Equations (10) and (12) give the energy dispersions for the surface states. It is seen that the surface states at  $k = 0$  exist if  $E_{lh}^{(I)}$  and  $E_{lh}^{(II)}$  are of different sign, which requires different signs of  $M^{(I)}$  and  $M^{(II)}$ .

For simplicity, we set  $C^{(n)} = 0$  and analyze the case  $S^{(n)} = -M^{(n)}$ . The latter for instance corresponds to the Kane fermions in unstrained HgCdTe crystals<sup>40,41</sup>. In this case, Eq. (12) can be reduced to

$$A (\hbar^2 v^2 k^2)^2 - B \hbar^2 v^2 k^2 + E^2 (E + M^{(I)})^2 (E + M^{(II)})^2 = 0, \quad (13)$$

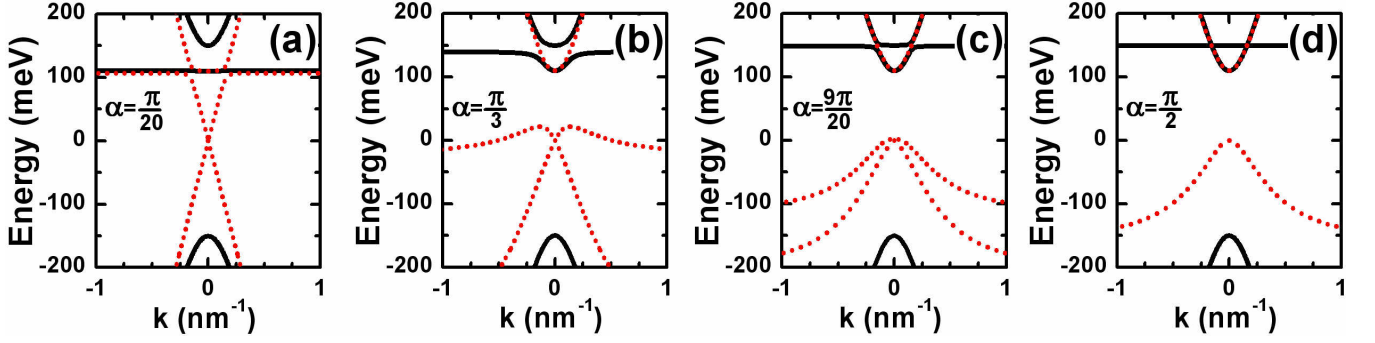


FIG. 2. (Color online) Dispersion of the bulk (solid black,  $k_z = 0$ ) and surface (dotted red) states as a function of  $k$  (where  $k^2 = k_x^2 + k_y^2$ ) for tensile strained film ( $S^{(II)} < -M^{(II)}$ ) with parameters of HgTe sandwiched between CdTe layers at different values of  $\alpha$ . The boundary is parallel to (001) crystallographic plane,  $S^{(II)} = 110$  meV. The value of  $\alpha = \pi/3$  corresponds to 6-band Kane Hamiltonian for band structure in HgCdTe crystals<sup>40,41</sup>.

where

$$A = \frac{(M^{(I)} - M^{(II)})^2}{4} \sin^4 \alpha + (E + M^{(I)})(E + M^{(II)}) \sin^2 \alpha,$$

$$B = (E^2 - M^{(I)}M^{(II)})(E + M^{(I)})(E + M^{(II)}) \sin^2 \alpha + (E + M^{(I)})^2(E + M^{(II)})^2. \quad (14)$$

One can see that for  $\alpha \neq 0$ , the energy of the surface states at  $k = 0$  has three different values  $-M^{(I)}$ , 0 and  $-M^{(II)}$ . At large values of  $k$ , the energy asymptotically tends to the values

$$E_{as\pm} = -\frac{M^{(I)} + M^{(II)}}{2} \pm \frac{M^{(I)} - M^{(II)}}{2} \cos \alpha, \quad (15)$$

which both are found from condition of  $A = 0$ . In the special case of  $\alpha = 0$ , i.e. in the absence of hybridization with a flat band, in addition to  $E = -M^{(I)}$  and  $E = -M^{(II)}$ , Eqs. (13) and (14) also give  $E = \pm \hbar v k$ .

Figure 1 shows the dispersion of bulk and surface states for different values of  $\alpha$  in the range  $(0, \pi/2]$  for an unstrained film of HgTe ( $\hbar v = 850$  meV·nm<sup>41</sup> and  $M^{(II)} = -150$  meV) embedded in CdTe layers ( $M^{(I)} = 450$  meV). Although the bulk dispersion remains the same for any values of  $\alpha$  ( $S^{(n)} = -M^{(n)}$ , see Eq. (5)), dispersion of the surface states strongly depends on hybridization with the flat bands in both materials. At small values of  $\alpha$  (see Fig. 1(a)), it consists of three branches  $E = E_{as+}$ ,  $E = \pm \hbar v k$  and  $E = E_{as-}$  anticrossing in the vicinity of the crossing points. In this case, the values of  $E_{as+}$  and  $E_{as-}$  are very close to  $-M^{(II)}$  and  $-M^{(I)}$ , respectively, since  $\cos \alpha \approx 1$  in Eq. (15). This picture can be also treated within the conventional degenerate perturbation approach.

With increasing of  $\alpha$ , the surface states for  $-M^{(I)} < E < -M^{(II)}$  are pushed away from the energies of the flat bulk bands in the materials at both sides of the boundary toward the regions where these bulk states are absent.

This is clearly represented by evolution of the asymptotic energies  $E_{as+}$  and  $E_{as-}$ , which are getting closer each other with  $\alpha$  as shown in Fig. 1(a-c). Note that dispersion of the surface states remains linear in the vicinity of the  $\Gamma$  point of the Brillouin zone. At specific value of  $\alpha = \pi/2$ , the asymptotic energies coincide both being equal to  $-(M^{(I)} + M^{(II)})/2$ , and the surface states become degenerate, see Fig. 1(d). The latter means the absence of odd-in- $k$  terms in their dispersion.

In addition to modification of the surface states in the range of  $-M^{(I)} < E < -M^{(II)}$ , for  $E > -M^{(II)}$  hybridization with the flat bulk bands also yields new "massive" branches in the regions above and below the bulk bands. Note that the lowest branch below  $-M^{(I)}$  in Fig. 1 is not shown. We refer to the upper "massive" surface states above the flat band as the *Dyakonov-Khaetskii* (DK) branch. Such DK branch is caused by the band inversion and, as seen from Fig. 1, is directly related to hybridization with the flat bulk band in HgTe.

The massive surface states at surface of HgTe crystal was first theoretically predicted in 1981 by Dyakonov and Khaetskii<sup>42</sup>. They derived analytically this branch by using Luttinger Hamiltonian for the  $\Gamma_8$  band<sup>43</sup> with an open boundary conditions. In 1985, existence of the localized states at the HgTe/CdTe interface was also predicted for the quantum wells<sup>44</sup> and superlattices<sup>45</sup>. Although the Luttinger Hamiltonian, used in Refs<sup>42,44</sup>, does not formally consider the inverted  $|\Gamma_6, \pm 1/2\rangle$  band, this Hamiltonian can be formally derived from the 6-band Kane Hamiltonian with the HgTe/CdTe interface by assuming  $M^{(II)} \rightarrow -\infty$  and  $M^{(I)} \rightarrow \infty$ . Thus, our "massive" surface states in Fig. 1 and solution of Dyakonov and Khaetskii<sup>42</sup> have both the same origin caused by hybridization with the bulk band.

Now we consider a bulk crystal, in which the flat band does not coincide with the bottom of conduction band, i.e.  $S^{(II)} \neq -M^{(II)}$ . The case of  $S^{(II)} < -M^{(II)}$  corresponds to external tensile biaxial strain, which opens a gap in HgTe, yielding 3D TI state<sup>23,24</sup>. The opposite case of  $S^{(II)} > -M^{(II)}$  is realized in the compres-

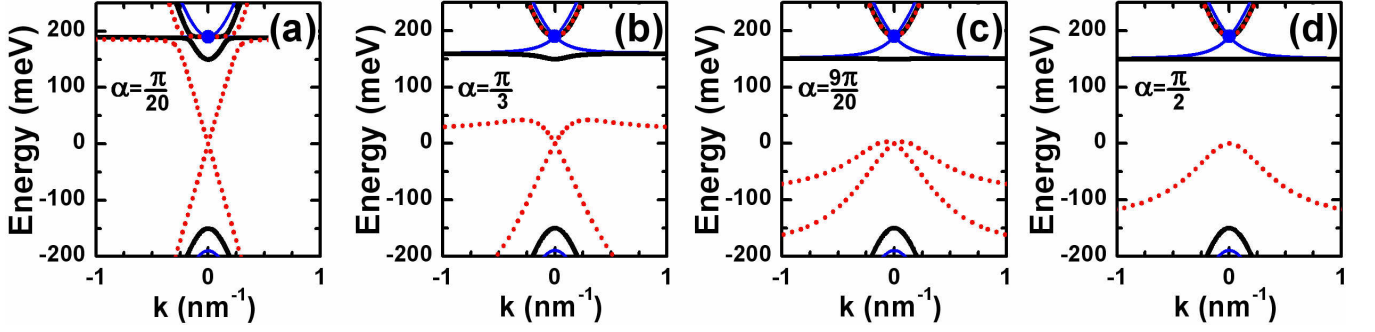


FIG. 3. (Color online) Dispersion of the bulk (solid black,  $k_z = 0$ ) and surface (dotted red) states as a function of  $k$  (where  $k^2 = k_x^2 + k_y^2$ ) for the bulk film with  $S^{(II)} > -M^{(II)}$  at different values of  $\alpha$ . The boundary is parallel to (001) crystallographic plane,  $S^{(II)} = 190$  meV. The solid blue curves show bulk dispersion at  $k_z = \pm k_D$ , where  $\hbar^2 v^2 k_D^2 = (S^{(II)})^2 - (M^{(II)})^2$ . Blue symbols represent projection of bulk Dirac nodes at  $\alpha \neq 0$  on the boundary surface. The value of  $\alpha = \pi/3$  corresponds to 6-band Kane Hamiltonian, which describes the band structure in real HgCdTe and  $\text{Cd}_3\text{As}_2$  crystals.

sively strained HgTe films<sup>27</sup> or in unstrained  $\text{Cd}_3\text{As}_2$  crystals<sup>28–31</sup>. As in previous case, we set  $C^{(n)} = 0$  and assume  $S^{(I)} = -M^{(I)}$  in CdTe layer.

Fig. 2 shows dispersion of the bulk and surface states at different values of  $\alpha$  in the  $(0, \pi/2]$  range for tensile strained HgTe film with  $S^{(II)} = 110$  meV bounded with CdTe. Note that now the energy dispersions are calculated numerically on the basis of Eq. (4) and Eqs. (10), (12) for the bulk and surface states, respectively. It is seen that energy of the bulk states and the value of a band-gap between the flat and conduction bands strongly depend on  $\alpha$ . The maximum gap is achieved in the absence of hybridization, while increasing of  $\alpha$  leads to a band-gap vanishing. The value of  $\alpha = \pi/2$  corresponds to a semimetal with circular nodal line at  $k_z = 0$  and  $k = k_N$ , where  $k_N^2 = 2M^{(II)}(M^{(II)} + S^{(II)})/(\hbar^2 v^2)$ .

As seen from Fig. 2, the picture of the surface states in tensile strained HgTe at different  $\alpha$  remains qualitatively the same, as in Fig. 1 for the unstrained film. The main difference is seen in the DK branch, which now exists in the band-gap for the bulk states at  $0 < \alpha \leq \pi/2$ . This is in agreement with the general topological arguments claiming that tensile strained HgTe is 3D TI with the gapless surface states<sup>23</sup>. However, these surface states can not be presented by massless Dirac fermions, as it is stated in some works (see, for instance, Refs.<sup>46–48</sup>). Fig. 2 clearly shows that the surface states in HgTe-based 3D TI are "massive" due to hybridization with heavy-hole  $|\Gamma_8, \pm 3/2\rangle$  band and represented by DK branch<sup>42</sup>.

In the opposite case of  $S^{(II)} > -M^{(II)}$ , the flat band crosses conduction band at certain points of the Brillouin zone at  $\alpha \neq 0$ <sup>28</sup> yielding a so-called 3D Dirac semimetal. At these points, the conduction and flat heavy-hole valence bands can be considered as two highly anisotropic and tilted cones<sup>29–31</sup>, whose nodes are located at  $k_x = k_y = 0$  and  $k_z = \pm k_D$  with  $k_D^2 = (S^2 - M^2)/(\hbar^2 v^2)$ , see Eq. (4). Note that at  $\alpha = 0$ , the crossing points are located at the sphere defined by

$\hbar^2 v^2 (k_x^2 + k_y^2 + k_z^2) = (S^2 - M^2)$ , and 3D Dirac semimetal does not arise.

Fig. 3 presents a picture of the bulk and surface states in the film with  $S^{(II)} > -M^{(II)}$  at different strength of hybridization with a flat band at  $S^{(II)} = 190$  meV. As for the previous case of  $S^{(II)} < -M^{(II)}$ , the energy dispersion of the bulk and surface states both depend on the values of  $\alpha$ . By compare figures 1, 2 and 3, one concludes that the surface states in the range of  $-M^{(I)} < E < -M^{(II)}$  do not change qualitatively at different position of the flat band, in contrast to the DK branch, whose bottom energy coincides with  $S^{(II)}$ . Interestingly, that dispersion of the surface states for all  $\alpha \neq 0$  starts from projection of the bulk Dirac nodes. The bulk band dispersion as a function of  $k$  at  $k_z = k_D$  is presented by the blue curves. Note that particular case of  $\alpha = \pi/3$  is in a good qualitative agreement with the picture of the surface states obtained from the first-principles band-structure calculations for  $\text{Cd}_3\text{As}_2$ <sup>29</sup> (see Fig. 3(a,b) therein).

One of the inherent characteristic of the surface states in Dirac semimetals is the existence of a pair of surface Fermi arcs connecting bulk Dirac nodes projected on the surface boundary. The arcs meet at a sharp corner or "kink" at the projected nodes. Such a kink is not allowed in a purely 2D metal, it is a special feature of the crystal symmetry-protected Weyl structure of the Dirac semimetals<sup>32</sup>. As the Dirac nodes are located along (001) crystallographic direction, the surface boundary parallel to (001) plane has no Fermi arcs.

## B. Surface states for the boundary parallel to (010) plane

Let us now briefly consider the surface states for the boundary containing both projections of bulk Dirac nodes at  $S^{(II)} > -M^{(II)}$ . For the boundary plane parallel to the  $x$ - $z$  plane and placed at  $y = 0$ , the



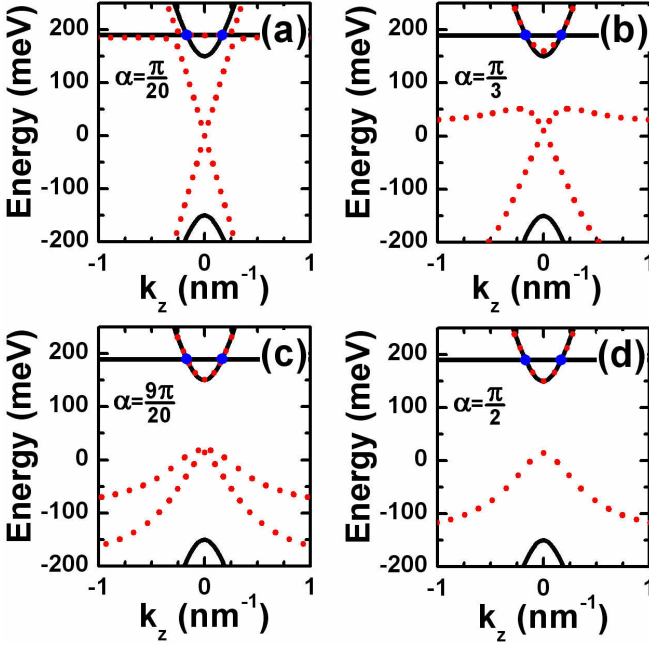


FIG. 4. (Color online) Dispersion of the bulk (solid black,  $k_x = k_y = 0$ ) and surface (dotted red,  $k_x = 0$ ) states as a function of  $k_z$  for the bulk film with  $S^{(II)} > -M^{(II)}$  with the boundary parallel to (010) crystallographic plane at different values of  $\alpha$ . As for Fig. 3, we assume  $S^{(II)} = 190$  meV. Blue symbols represent position of bulk Dirac nodes at  $\alpha \neq 0$ .

wave-function of the surface states has the form  $\Phi_{1,2}^{(I)} \sim \exp(\lambda_y^{(I)} y) \exp(ik_x x + ik_z z)$  for  $y < 0$  and  $\Phi_{1,2}^{(II)} \sim \exp(-\lambda_y^{(II)} y) \exp(ik_x x + ik_z z)$  for  $y > 0$ . With these functions, Eq. (6) yields the following values of  $\lambda_y^{(I)}$  and  $\lambda_y^{(II)}$ :

$$\lambda_y^{(n)} = \sqrt{k_x^2 + \frac{k_z^2 - \frac{E_c^{(n)} E_{lh}^{(n)}}{\hbar^2 v^2}}{1 + \frac{E_{lh}^{(n)} - E_{hh}^{(n)}}{E_{hh}^{(n)}} \sin^2 \alpha}}, \quad (16)$$

where the index  $n = I, II$  corresponds to  $y < 0$  and  $y > 0$ , respectively.

Integration of Eq. (6) across the small region of  $y = 0$  gives the continuity function across the junction:

$$\begin{pmatrix} \Phi_1 \\ \Phi_2 \end{pmatrix}, \quad \begin{pmatrix} R_+ \frac{\partial}{\partial y} + R_- k_x & k_z \frac{\cos \alpha}{E_{lh}} \\ k_z \frac{\cos \alpha}{E_{lh}} & R_+ \frac{\partial}{\partial y} - R_- k_x \end{pmatrix} \begin{pmatrix} \Phi_1 \\ \Phi_2 \end{pmatrix}, \quad (17)$$

where  $R_+$  and  $R_-$  are function of  $E$  and  $\alpha$ :

$$R_{\pm}(E) = \frac{\cos^2 \alpha}{E_{lh}(E)} \pm \frac{\sin^2 \alpha}{E_{hh}(E)}. \quad (18)$$

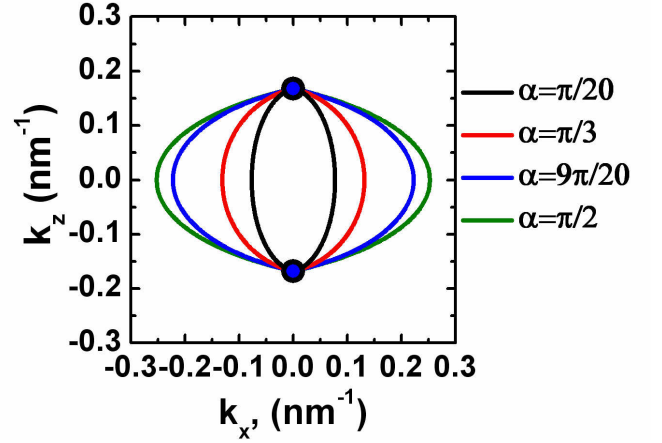


FIG. 5. (Color online) Energy contour for the surface states at  $E = S^{(II)}$  for the boundary parallel to (010) crystallographic plane in the film with  $S^{(II)} > -M^{(II)}$ . Blue symbols represent position of bulk Dirac nodes at  $\alpha \neq 0$ . Note that Dirac nodes and Fermi arcs do not exist at  $\alpha = 0$ .

Applying these boundary conditions to  $\Phi_{1,2}^{(I)}$  and  $\Phi_{1,2}^{(II)}$ , the secular equation for the non-trivial solution leads to

$$\begin{aligned} & \left( \lambda_y^{(I)} R_+^{(I)}(E) + \lambda_y^{(II)} R_+^{(II)}(E) \right)^2 = \\ & = k_z^2 \left( \frac{1}{E_{lh}^{(II)}} - \frac{1}{E_{lh}^{(I)}} \right)^2 \cos^2 \alpha + \\ & + k_x^2 \left( R_-^{(II)}(E) - R_-^{(I)}(E) \right)^2. \quad (19) \end{aligned}$$

Numerical solution of Eqs (16), (18) and (19) gives the energy dispersion and energy contours of the surface states for the boundary parallel to the (010) crystallographic plane.

Fig. 4 shows dispersions of the bulk and surface states as a function of  $k_z$  for the bulk film with  $S^{(II)} > -M^{(II)}$  and (010) surface boundary. Here, we set  $C^{(n)} = 0$ ,  $S^{(I)} = -M^{(I)}$ ,  $S^{(II)} = 190$  meV and assume  $k_x = k_y = 0$ . As for the (001) boundary, the picture of surface states for all  $\alpha$  values consists of two branches above and below the bottom of conduction band at  $E = -M^{(II)}$ . As the upper massive branch for  $\alpha = \pi/3$  can be also obtained from the model used by Dyakonov and Khaetskii<sup>42</sup>, we also call it the DK branch. Such DK branch for all  $\alpha \neq 0$  crosses the bulk dispersion precisely at the Dirac nodes. This results from the fact that two separated Dirac nodes are connected by the topological surface states<sup>32</sup>. Interestingly, the surface states for  $\alpha = \pi/3$  are also consistent with the first-principles band-structure calculations performed for  $\text{Cd}_3\text{As}_2$ <sup>29</sup> (see Fig. 3(c,d) therein).

Fig. 5 provides energy contours for the surface states at  $E = S^{(II)}$  at different strength of hybridization with the flat band. In contrast to the (001) boundary, for which the energy contour of the surface states reduced to a point, the nontrivial surface states at the (010) boundary are clearly visible. Its Fermi surface at  $E = S^{(II)}$  is

composed of two Fermi arcs with the kinks at the projected bulk Dirac nodes. As seen from Fig. 5, the length of Fermi arcs depends on the values of  $\alpha$ . This means that the period of quantum oscillations originated from cyclotron orbits weaving together Fermi arcs and chiral bulk states<sup>32</sup>, should also depend on the hybridization strength. These quantum oscillations have been recently observed in magnetotransport measurements performed on  $\text{Cd}_3\text{As}_2$ <sup>33,34</sup>.

#### IV. SUMMARY

In conclusion, we have performed theoretical studies of hybridization between topological surface states and non-topological bulk flat band. Depending on hybridization strength, our model linear in quasimomentum interpolates between 3D BHZ model with decoupled flat band and 6-band Kane Hamiltonian. We have shown that hybridization with a bulk band in HgTe transforms initial Dirac-like surface states into two branches below the flat band and above the edge of conduction band. Dispersion of the lower branch depends on hybridization strength, while the upper branch, theoretically predicted

in 1981 by Dyakonov and Khaetskii<sup>42</sup> remains "massive" for any hybridization strength. By varying position of the flat band relatively to the conduction band edge, we have obtained a picture of topological surface states in 3D TI and Dirac semimetals in strained HgTe films and  $\text{Cd}_3\text{As}_2$  crystals. In particular, we have shown that surface states of tensile strained HgTe 3D TI are always massive and cannot be considered as Dirac fermions<sup>46-48</sup>. For the compressively strained HgTe and  $\text{Cd}_3\text{As}_2$ , we have demonstrated that the length of Fermi arcs, which connect bulk Dirac nodes projected on the surface boundary, also depends on the hybridization strength. For particular values of hybridization strength, corresponding to 6-band Kane Hamiltonian, our picture of the surface states is in good qualitative agreement with the previous first-principles calculations performed for  $\text{Cd}_3\text{As}_2$ <sup>29</sup>.

#### ACKNOWLEDGMENTS

This work was supported by the CNRS through LIA "TeraMIR", by the French Agence Nationale pour la Recherche (Dirac3D project), and by the Russian Science Foundation (Grant No. 16-12-10317).

- 
- \* frederic.teppe@umontpellier.fr
- <sup>1</sup> C. L. Kane and E. J. Mele, Phys. Rev. Lett. **95**, 226801 (2005).
  - <sup>2</sup> F. D. M. Haldane, Phys. Rev. Lett. **61**, 2015 (1988).
  - <sup>3</sup> L. Fu, C. L. Kane, and E. J. Mele, Phys. Rev. Lett. **98**, 106803 (2007).
  - <sup>4</sup> J. E. Moore and L. Balents, Phys. Rev. B **75**, 121306 (2007).
  - <sup>5</sup> R. Roy, Phys. Rev. B **79**, 195322 (2009).
  - <sup>6</sup> M. Z. Hasan and C. L. Kane, Rev. Mod. Phys. **82**, 3045 (2010).
  - <sup>7</sup> X.-L. Qi and S.-C. Zhang, Rev. Mod. Phys. **83**, 1057 (2011).
  - <sup>8</sup> B. A. Bernevig, T. L. Hughes, and S.-C. Zhang, Science **314**, 1757 (2006).
  - <sup>9</sup> M. König, S. Wiedmann, C. Brüne, A. Roth, H. Buhmann, L. W. Molenkamp, X.-L. Qi, and S.-C. Zhang, Science **318**, 766 (2007).
  - <sup>10</sup> C. Liu, T. L. Hughes, X.-L. Qi, K. Wang, and S.-C. Zhang, Phys. Rev. Lett. **100**, 236601 (2008).
  - <sup>11</sup> I. Knez, R.-R. Du, and G. Sullivan, Phys. Rev. Lett. **107**, 136603 (2011).
  - <sup>12</sup> S. S. Krishtopenko and F. Teppe, Sci. Adv. **4**, eaap7529 (2018).
  - <sup>13</sup> S. S. Krishtopenko, S. Ruffenach, F. Gonzalez-Posada, G. Boissier, M. Marcinkiewicz, M. A. Fadeev, A. M. Kadykov, V. V. Rumyantsev, S. V. Morozov, V. I. Gavrilenko, C. Consejo, W. Desrat, B. Jouault, W. Knap, E. Tournié, and F. Teppe, Phys. Rev. B **97**, 245419 (2018).
  - <sup>14</sup> S. Wu, V. Fatemi, Q. D. Gibson, K. Watanabe, T. Taniguchi, R. J. Cava, and P. Jarillo-Herrero, Science **359**, 76 (2018).
  - <sup>15</sup> Y. Xia, D. Qian, D. Hsieh, L. Wray, A. Pal, H. Lin, A. Bansil, D. Grauer, Y. S. Hor, R. J. Cava, and M. Z. Hasan, Nature Phys. **5**, 398 (2009).
  - <sup>16</sup> H. Zhang, C.-X. Liu, X.-L. Qi, X. Dai, Z. Fang, and S.-C. Zhang, Nature Phys. **5**, 438 (2009).
  - <sup>17</sup> Y. L. Chen, J. G. Analytis, J.-H. Chu, Z. K. Liu, S.-K. Mo, X. L. Qi, H. J. Zhang, D. H. Lu, X. Dai, Z. Fang, S. C. Zhang, I. R. Fisher, Z. Hussain, and Z.-X. Shen, Science **325**, 178 (2009).
  - <sup>18</sup> D. Hsieh, Y. Xia, L. Wray, D. Qian, A. Pal, J. H. Dil, J. Osterwalder, F. Meier, G. Bihlmayer, C. L. Kane, Y. S. Hor, R. J. Cava, and M. Z. Hasan, Science **323**, 919 (2009).
  - <sup>19</sup> L. Fu, Phys. Rev. Lett. **106**, 106802 (2011).
  - <sup>20</sup> T. H. Hsieh, H. Lin, J. Liu, W. Duan, A. Bansil, and L. Fu, Nat. Commun. **3**, 982 (2012).
  - <sup>21</sup> P. Dziawa, B. J. Kowalski, K. Dybko, R. Buczek, A. Szczerbakow, M. Szot, E. Lusakowska, T. Balasubramanian, B. M. Wojek, M. H. Berntsen, O. Tjernberg, and T. Story, Nat. Mater. **11**, 1023 (2012).
  - <sup>22</sup> Y. Okada, M. Serbyn, H. Lin, D. Walkup, W. Zhou, C. Dhital, M. Neupane, S. Xu, Y. J. Wang, R. Sankar, F. Chou, A. Bansil, M. Z. Hasan, S. D. Wilson, L. Fu, and V. Madhavan, Science **341**, 1496 (2013).
  - <sup>23</sup> L. Fu and C. L. Kane, Phys. Rev. B **76**, 045302 (2007).
  - <sup>24</sup> C. Brüne, C. X. Liu, E. G. Novik, E. M. Hankiewicz, H. Buhmann, Y. L. Chen, X. L. Qi, Z. X. Shen, S. C. Zhang, and L. W. Molenkamp, Phys. Rev. Lett. **106**, 126803 (2011).
  - <sup>25</sup> O. E. Raichev, Phys. Rev. B **85**, 045310 (2012).
  - <sup>26</sup> S. S. Krishtopenko and F. Teppe, Phys. Rev. B **97**, 165408 (2018).
  - <sup>27</sup> P. Leubner, L. Lunczer, C. Brüne, H. Buhmann, and L. W. Molenkamp, Phys. Rev. Lett. **117**, 086403 (2016).

- <sup>28</sup> J. Bodnar, Proc. III Conf. Narrow-Gap Semiconductors, Warsaw, edited by J. Rauluszkiewicz, M. Górská, and E. Kaczmarek (Elsevier, 1977) pp. 311, see also arXiv:1709.05845 .
- <sup>29</sup> Z. Wang, H. Weng, Q. Wu, X. Dai, and Z. Fang, Phys. Rev. B **88**, 125427 (2013).
- <sup>30</sup> A. Akrap, M. Hakl, S. Tchoumakov, I. Crassee, J. Kuba, M. O. Goerbig, C. C. Homes, O. Caha, J. Novák, F. Teppe, W. Desrat, S. Koohpayeh, L. Wu, N. P. Armitage, A. Nateprov, E. Arushanov, Q. D. Gibson, R. J. Cava, D. van der Marel, B. A. Piot, C. Faugeras, G. Martinez, M. Potemski, and M. Orlita, Phys. Rev. Lett. **117**, 136401 (2016).
- <sup>31</sup> W. Desrat, S. S. Krishtopenko, B. A. Piot, M. Orlita, C. Consejo, S. Ruffenach, W. Knap, A. Nateprov, E. Arushanov, and F. Teppe, Phys. Rev. B **97**, 245203 (2018).
- <sup>32</sup> A. C. Potter, I. Kimchi, and A. Vishwanath, Nat. Commun. **5**, 5161 (2014).
- <sup>33</sup> P. J. W. Moll, N. L. Nair, T. Helm, A. C. Potter, I. Kimchi, A. Vishwanath, and J. G. Analytis, Nature **535**, 266 (2016).
- <sup>34</sup> C. Zhang, A. Narayan, S. Lu, J. Zhang, H. Zhang, Z. Ni, X. Yuan, Y. Liu, J.-H. Park, E. Zhang, W. Wang, S. Liu, L. Cheng, L. Pi, Z. Sheng, S. Sanvito, and F. Xiu, Nat. Commun. **8**, 1272 (2017).
- <sup>35</sup> D. L. Bergman and G. Refael, Phys. Rev. B **82**, 195417 (2010).
- <sup>36</sup> Y.-T. Hsu, M. H. Fischer, T. L. Hughes, K. Park, and E.-A. Kim, Phys. Rev. B **89**, 205438 (2014).
- <sup>37</sup> C. Seibel, H. Bentmann, J. Braun, J. Minár, H. Maaß, K. Sakamoto, M. Arita, K. Shimada, H. Ebert, and F. Reinert, Phys. Rev. Lett. **114**, 066802 (2015).
- <sup>38</sup> J. D. Malcolm and E. J. Nicol, Phys. Rev. B **92**, 035118 (2015).
- <sup>39</sup> A. Raoux, M. Morigi, J.-N. Fuchs, F. Piéchon, and G. Montambaux, Phys. Rev. Lett. **112**, 026402 (2014).
- <sup>40</sup> M. Orlita, D. M. Basko, M. S. Zholudev, F. Teppe, W. Knap, V. I. Gavrilenko, N. N. Mikhailov, S. A. Dvoret-skii, P. Neugebauer, C. Faugeras, A.-L. Barra, G. Martinez, and M. Potemski, Nature Phys. **10**, 233 (2014).
- <sup>41</sup> F. Teppe, M. Marcinkiewicz, S. S. Krishtopenko, S. Ruffenach, C. Consejo, A. M. Kadykov, W. Desrat, D. But, W. Knap, J. Ludwig, S. Moon, D. Smirnov, M. Orlita, Z. Jiang, S. V. Morozov, V. Gavrilenko, N. N. Mikhailov, and S. A. Dvoret-skii, Nat. Commun. **7**, 12576 (2016).
- <sup>42</sup> M. I. Dyakonov and A. V. Khaetskii, JETP Lett. **33**, 110 (1981).
- <sup>43</sup> J. M. Luttinger, Phys. Rev. **102**, 1030 (1956).
- <sup>44</sup> Y. R. Lin-Liu and L. J. Sham, Phys. Rev. B **32**, 5561 (1985).
- <sup>45</sup> Y.-C. Chang, J. N. Schulman, G. Bastard, Y. Guldner, and M. Voos, Phys. Rev. B **31**, 2557 (1985).
- <sup>46</sup> D. A. Kozlov, D. Bauer, J. Ziegler, R. Fischer, M. L. Savchenko, Z. D. Kvon, N. N. Mikhailov, S. A. Dvoret-sky, and D. Weiss, Phys. Rev. Lett. **116**, 166802 (2016).
- <sup>47</sup> C. Thomas, O. Crauste, B. Haas, P.-H. Jouneau, C. Bäuerle, L. P. Lévy, E. Orignac, D. Carpentier, P. Ballet, and T. Meunier, Phys. Rev. B **96**, 245420 (2017).
- <sup>48</sup> P. Noel, C. Thomas, Y. Fu, L. Vila, B. Haas, P.-H. Jouneau, S. Gambarelli, T. Meunier, P. Ballet, and J. P. Attané, Phys. Rev. Lett. **120**, 167201 (2018).